Ag-Mediated Charge Transport during Metal-Assisted Chemical Etching of Silicon Nanowires

Nadine Geyer,*,[†] Bodo Fuhrmann,[‡] Hartmut S. Leipner,[‡] and Peter Werner[†]

[†]Max Planck Institute of Microstructure Physics, Weinberg 2, D-06120 Halle, Germany

[‡]Interdisciplinary Center of Materials Science, Martin Luther University, Halle-Wittenberg Heinrich-Damerow-Straße 4, D-06120 Halle, Germany

S *Supporting Information*

ABSTRACT: The charge transport mechanism during metal-assisted chemical etching of Si nanowires with contiguous metal films has been investigated. The experiments give a better insight how the charges and reaction products can penetrate to the etching front. The formation of a layer of porous Si between the metal film and the bulk Si is a prerequisite for the etching process. The electronic holes (positive charges) necessary for the etching of porous Si are generated at the surface of the metal in contact with the oxidative agent. Because of the insulating character of the thin walls of the porous Si, the transport of the electronic holes through this layer is not possible. Instead, it is found that the transport of electronic holes proceeds primarily by means of the Ag/Ag^+ redox pair circulating in the electrolyte and diffusing through the etched pores in the Si. The charge transport occurs without the ionic contribution at the positions where the metal is in direct contact with the Si. Here, an electropolishing process takes place, leading to an extensive removal of the Si and sinking in of the film into the Si substrate.

KEYWORDS: metal-assisted chemical etching, silicon nanowires, etching model, porous silicon, Ag/Ag^+ redox mediator, charge transport
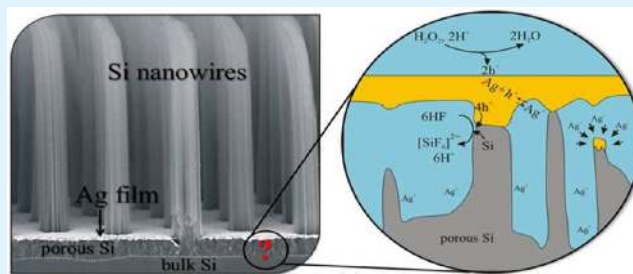
INTRODUCTION

Nanostructures of semiconducting materials are of great interest for both fundamental research and technological applications. They show novel optical, electrical and mechanical properties, due to, for example, quantum effects and high surface area to volume ratio. In particular, quasi one-dimensional nanostructures, so-called nanowires (NWs), are being studied intensively, because of their potential applications in the field of electronics,[1,2] optoelectronics,[3] thermoelectrics,[4] and photovoltaics,[5−7] as well as for biological and chemical sensors.[8,9] However, for their technological applications, the precise tuning of the properties of the NWs is fundamental. For this purpose, NWs can be obtained by either bottom-up growth (e.g., molecular beam epitaxy or chemical vapor deposition) or a top-down etching.[10] The mostly used top-down approach involves reactive ion etching of patterned substrates. However, this method may lead to an extensive damage of the crystal structure and surface morphology. To overcome this drawback, one resorted in recent years to so-called metal-assisted chemical etching (MACE).[11−14] This approach comprises two steps. First, a lithographically structured noble metal film (Ag, Au, Pt, Pd) is deposited on the substrate. Second, the etching in a hydrofluoric-acid-based solution (HF + oxidative agent) is performed. All procedures can be carried out in a chemical lab without expensive equipment which makes this method potentially cheaper and applicable for mass production in the industrial processes. Because of the simplicity of this technique, MACE has recently gained popularity for the production of NWs. Whereas the fabrication of NWs using metal films has been successfully demonstrated, the corresponding physical and chemical mechanisms, in particular the mass and charge transport during the formation of NWs, are still not well understood on a microscopic scale, and no suitable models exist. The aim of this work is to systematically contribute to the fundamental understanding of these issues.

PRELIMINARIES

A substantial work has been devoted to the understanding of MACE taking advantage of isolated metal particles[15−17] and we take these experiments as the starting point in our considerations. In 2000, Li and Bohn observed in their studies that thin noble metal films (thickness <10 nm) or metal particles such as Au, Pt, or from an Au/Pd alloy, sputtered on a (100) Si surface, show a catalytic effect in presence of HF and an oxidative agent like H_2O_2 or HNO_3 leading to the formation of channels in the silicon substrate.[18] Later on, the development of porous Si (pSi) was observed by Chartier et al. at the wall of the channels and underneath the metal particle.[19] It brought
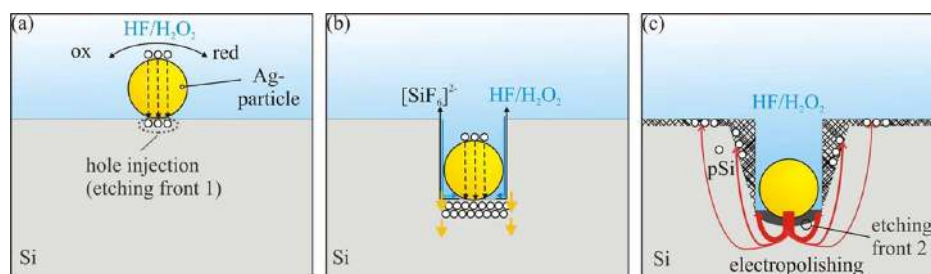
**Figure 1.** Commonly adopted model of MACE with isolated metal particles. In the presence of the HF/H$_2$O$_2$ solution the particles catalyze the ablation of Si leading to the formation of cylindrical channels in the substrate. (a) Reduction of H$_2$O$_2$ at the surface of the metal and injection of electronic holes into the Si substrate, (b) oxidation of the Si surface, (c) diffusion of electronic holes leading automatically to the two regimes known from anodic etching: directly beneath the metal particle, the electronic holes diffuse into the Si and then to the surface. Directly beneath the particle, the current density reaches its maximum and is high enough for an electropolishing process to occur (regime A). With an increasing distance from the metal particle, the current density decreases. Only porous Si is formed at the walls of the channel (regime B).

them to the conclusion that the processes underlying MACE do not differ substantially from those governing the well-studied anodic etching.[25,26] Following this analogy, they explained the MACE as two concurrent processes leading to the ablation of Si, namely (i) the formation of pSi and (ii) the electropolishing of Si. Both depend crucially on the generation and transport of electronic holes, but differ with respect to their local current densities. In MACE, the electronic holes are generated through redox reactions at the interface of the metal particle and the electrolyte. According to eq 1, the metal catalyzes the reduction of the oxidizing agent like H$_2$O$_2$ which subsequently injects electronic holes into the Si surface directly beneath the metal particle, see Figure 1a.

$$H_2O_2 + 2H^+ \rightarrow 2H_2O + 2h^+ \tag{1}$$
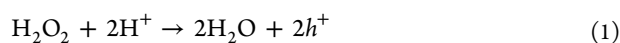
The open space around the particle allows the electrolyte to penetrate easily to the etching front, Si is locally oxidized and dissolved by HF. Consequently, the particle sinks into the formed channel, see Figure 1b. The geometry of the process leads automatically to the two regimes observed in anodic etching, see Figure 1c. Directly beneath the metal particle, the current density of holes reaches its maximum and becomes high enough for electropolishing to occur (regime A: tetravalent dissolution); Si is extensively removed there. This is how the channels are formed. In the literature, two different tetravalent oxidation reactions of Si are suggested: (RI) The direct dissolution of Si in tetravalent state[18,20,21]

$$Si + 4h^+ + 4HF \rightarrow SiF_4 + 4H^+ \tag{2}$$

$$SiF_4 + 2HF \rightarrow H_2SiF_6 \tag{3}$$
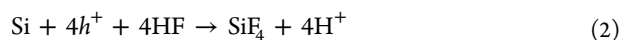
(RII) Oxidation of Si followed by the dissolution of the oxide[22−24]

$$Si + 2H_2O + 4h^+ \rightarrow SiO_2 + 4H^+ \tag{4}$$

$$SiO_2 + 6HF \rightarrow H_2SiF_6 + 2H_2O \tag{5}$$
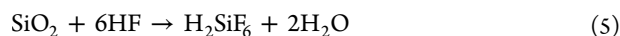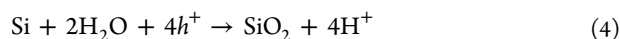
With increasing distance from the metal particle, the current density decreases, as required by the geometry, and the Si is removed only locally, leading to the formation of the pSi walls (regime B: divalent dissolution), see Figure 1c. The direct dissolution of Si in divalent state beneath the metal particle is described by Chartier et al.[19]

$$Si + 4HF_2^- + 2h^+ \rightarrow SiF_6^{(2-)} + 2HF + H_2\uparrow \tag{6}$$
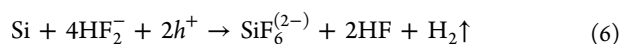
As indicated above, the fabrication of NWs by MACE necessitates metal films with openings. Although some similarities between etching with particles and with contiguous films can be expected, the latter technique exhibits several distinctive features pointing to alternative microscopic mechanisms involved, previously not discussed in the literature. The closed topology of the film hinders the access of the electrolyte to the etching front and the question of how the mass transport takes place arises. As we have shown recently, the mass transport occurs in a layer of mesoporous Si formed during etching beneath the metal film. The electrolyte penetrates through the lithographic openings and diffuses through the pores of the pSi layer to dissolve the oxidized Si. Furthermore, Geyer et al. observed that the massive ablation of the oxidized Si takes place only in direct contact with the metal, which is responsible for the formation of NWs.[27]

However, the nature of the charge transport still remains unclear. According to Lehmann and Gösele, no charge transport takes place through the pSi, due to the formation of a space charge region in the pore walls.[28] In the case of anodic etching, the holes originating from the application of an external voltage are injected from the backside of the Si wafer. In this case, the insulating nature of the pSi leads to the termination of the etching process after a certain time period. In contrast, the holes enter during MACE from the other side, i.e., through the contact with the metal. It seems that the electronic holes are able to penetrate through the porous layer, since it has been experimentally observed that the pSi layer continuously grows and is etched away. Clearly, besides the etching front forming directly between the metal and the Si surface (etching front 1), a second etching front between porous and bulk Si (etching front 2) has to be considered. Therefore, a suitable model of MACE with contiguous metal films must be able to explain the following issues: (i) What are the microscopic mechanisms that are responsible for the formation of the pSi layer? (ii) How does the charge transport through the layer proceed? (iii) Why is the direct contact with the metal necessary for the ablation of Si? (iv) How to resolve the apparent contradiction that the dissolution destroys the contact between Ag and Si necessary for the dissolution? We have performed a series of systematic experiments to shine light on these issues. The results are presented in the next sections followed by a summary presenting the charge transport model.

■ RESULTS

Figure 2a shows exemplarily SiNWs fabricated according to the procedure described in the methodical section. The morphol-
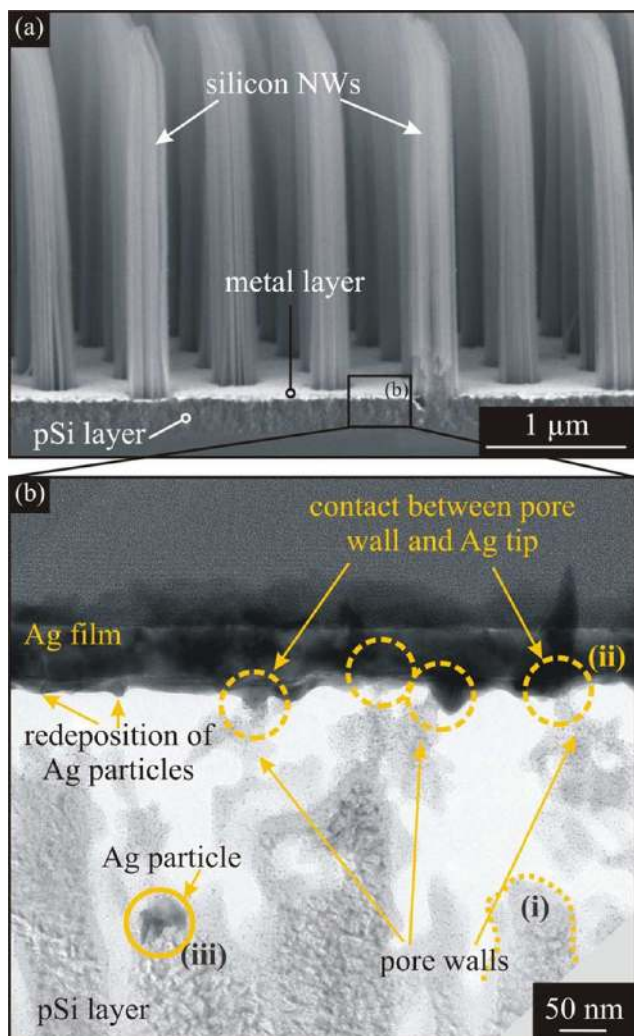
Figure 2. Patterning of a Si substrate with ordered SiNWs: (a) cross-section SEM image of SiNWs showing the typical porous layer beneath the Ag film, (b) TEM image of the pSi layer underneath the Ag film. The closed Ag film is composed of the original Ag layer and redeposited Ag particles. The images show pore walls (marked with (i)) connected with small Ag particles growing from the Ag film to the pore wall (marked with (ii)). Furthermore, isolated Ag clusters in the pSi appear (marked with (iii)).

ogy of the NWs has been characterized thoroughly. To allow a comparison of the results in the following experiments, all structures presented have been fabricated using highly n- as well as p-doped Si substrates. In all cases the doping level was kept at 1×10^{19} cm^{-3}. Anticipating the experiments presented below, we remark here briefly that the results presented in the paper do not depend on the type of the dopant.

The cross-section of the NW array demonstrates clearly that a porous layer directly beneath the Ag layer is formed. The growth rate of the pSi layer depends strongly on the doping level of the Si substrate used. Nevertheless, the pSi layer was found as well as for slightly and for highly doped Si substrates. The TEM image of Figure 2b shows the detailed morphology of the area beneath the Ag film, that means the structure of the

etching front 1. The film (dark area) is closed. The porous layer below consists (in analogy to mesoporous anodically etched Si) of pores and pore walls (marked with (i)). It can be observed, that the Ag film undergoes a cyclic formation and redeposition of metal. Ag dissolves during the etching, and single Ag particles redeposit on the film and on different places in the network of pores. Interestingly, small Ag droplets may form in direct contact to the tips of the pore walls (marked with (ii)). Some Ag droplets are also found deeper in the pSi (marked with (iii)). The role and physical mechanisms of the cyclic dissolution and redeposition of Ag is investigated below in a series of controlled experiments.

All experiments feature the following series of layers formed during etching: bulk Si, porous layer, and the Ag film on top. The porosity results in a passivation by quantum confinement and prevents any current flow through the porous layer, a fact well-known from anodic etching. Here, the question arises: Why does the pSi layer expands during the etching, and how can the electronic holes diffuse from the metal contact to the bulk Si-pSi interface (etching front 2)? Furthermore, is the direct electric contact of metal and Si necessary, as proposed in the literature?[19] The charge transport must proceed according to a different mechanism. To investigate this issue, we performed the following experiment. We introduced a layer of insulating and HF-inert material (photoresist) between the metal and the Si substrate. No charge transport is possible through the insulating material. To be specific, a photoresist stripe mask prepared lithographically was deposited on the surface of the Si substrate. A massive Ag wire (diameter: 0.5 mm) playing the role of the catalyst was placed on the photoresist mask, see Figure 3a. The distance between the wire and the Si substrate is determined by the thickness of the photoresist (width: 30 μm, thickness: 1 μm). The Ag wire expands only over a part of the sample. Figure 3(b-e) shows exemplarily BSE images of the system after 10 min etching. The black area is the photoresist. The areas in direct contact with Ag wire (Figure 3b, c) and far away from the wire (Figure 3d, e) differ significantly. In the top-view image of the area close to the wire see Figure 3b) a formation of Ag dendrites (white areas in BSE image) took place, accompanied by a massive ablation of pSi beneath the dendrites. This is confirmed by the corresponding cross-section BSE image of the area between the photoresist stripes (see Figure 3c). The formation of dendrites does not occur far away from the wire (see Figure 3d). Instead, a relatively thick porous layer is found between the photoresist stripes (see Figure 3e). Nearby the massive Ag wire the thickness of the pSi layer amounts to about 400 nm, while the pSi layer areas far away from the wire show a thickness of 1.9 μm.

The phenomenon of the observed Ag dissolution and redeposition can be compared with the etching of Si substrates containing a AgNO$_3$ solution.[29] In this case, there is also no direct contact between the Si substrate and the catalyst. The Ag is only present as ions, as in the present case. Because the Ag$^+$ ions feature a higher redox potential than the Si, the reduction of Ag$^+$ occurs and elementary Ag is deposited on the Si surface.[16] The deposited silver generates under the action of H$_2$O$_2$ the electronic holes necessary for the dissolution of Si. The experiment proves that the direct contact between the Si substrate and the metal is not necessary for MACE. The charge transport takes place via the redox reaction Ag $\leftrightarrow$Ag$^+$. The detailed explanation will be given in the discussion part.
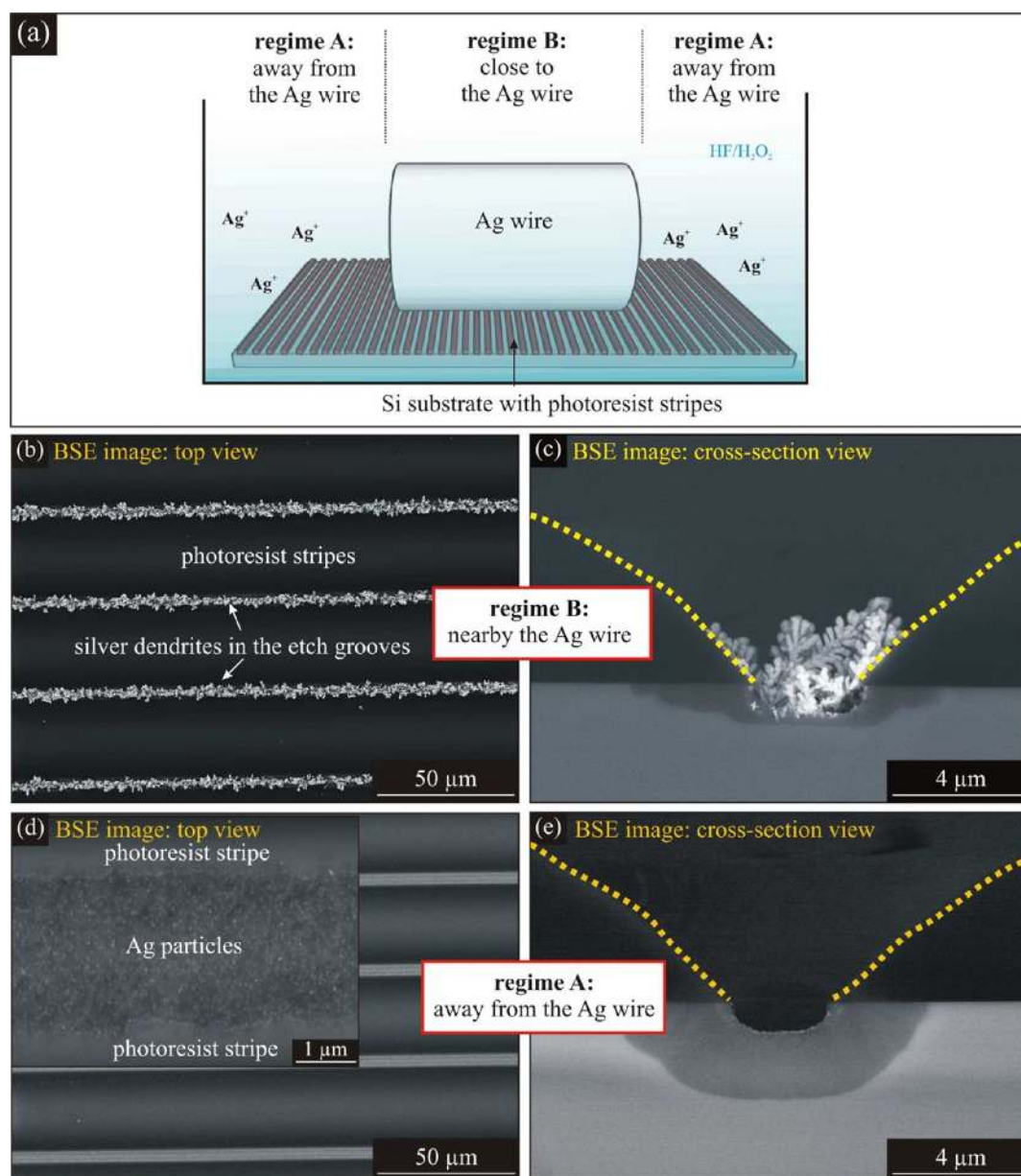
Figure 3. (a) Experimental setup for the investigation of the electronic transport in the MACE process. The Si substrate is masked with stripes of photoresist, preventing a massive Ag wire from the direct contact with the Si. The wire does not stretch over the whole sample, and two regimes can be discerned. (b) Regime B directly beneath the wire is characterized by a high concentration of Ag^+ ions. In the spaces between the stripes, a deposition of dendritic elemental Ag occurs. (c) Porous Si is extensively electropolished here. The yellow lines mark the borders of the photoresist. (d) Regime A away from the wire is characterized by the formation of pSi associated with (e) a low density of Ag^+.

The appearance of two regimes in the experiment presented bears again the analogy to the anodic etching. The concentration of Ag^+ varies as a function of the distance from the wire. Directly beneath the metal it reaches its maximum. Consequently, elementary Ag builds up and the electropolishing of Si takes place (regime B). Further away, the concentration drops and only pSi forms (regime A).

To investigate the etching behavior with different Ag^+ concentrations more precisely, we etched bare Si substrates in the etching solution for MACE mentioned in the experimental part. Additionally, a certain amount of Ag+ ions was added in the form of an $AgNO_3$ solution (0.18 μmol/L and 18 μmol/L). The formation of pSi during etching is visualized in Figure 4 in SE and corresponding BSE images. In the case of a 0.18 μmol/L concentration, the thickness of the pSi amounts to 300 nm

and for the amount of 18 μmol/L the thickness is 3 μm. In the case of the 18 μmol/L, the formation of Ag particles and pores in the substrate is clearly seen in the corresponding BSE image. For slightly doped Si substrate, the porous layer is also formed, but in contrast to the highly doped Si, its thickness is much smaller (see Figure SI 1 in the Supporting Information). The result of these experiments confirms the conclusion drawn by the previous experiments with a massive Ag wire. In the presence of a low Ag^+ ion concentration, only pSi is formed, whereas a higher Ag^+ ion density results in the formation of elemental Ag clusters leading to the etching of channels in the Si substrate. In this case, the current density becomes high enough for electropolishing of the Si to take place, in analogy to anodic etching. The formation of pSi takes place wherever the
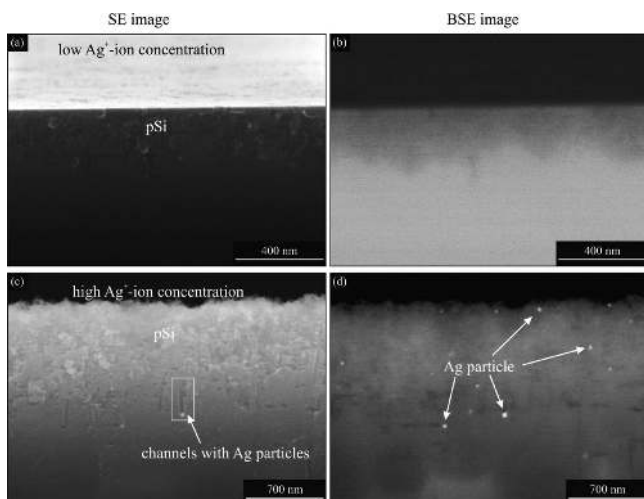
Figure 4. SE and BSE images of unstructured Si substrates (B-doped Si (100)-wafer, 10^{19} cm^{-3}) etched with the HF/H$_2$O$_2$ solution with an addition of small varying concentration of Ag$^+$ ions: (a,b) 0.18 μ mol/L, (c,d) 18 μmol/L. For the low concentration only pSi forms, whereas for higher concentrations, Ag particles appear incorporated into the structure of etched pores.

Ag$^+$ ions appear, but the electropolishing occurs only in direct contact with the metal catalyst.

To finally confirm that the Ag$^+$ ions play a decisive role in the charge transport and in the formation of pSi, we carried out the following experiment. Ag$^+$ ions are eliminated by adding hydrochloric acid (HCl) after 10 min etching. The results are presented in Figure 5. The Figure 5a shows the experiment
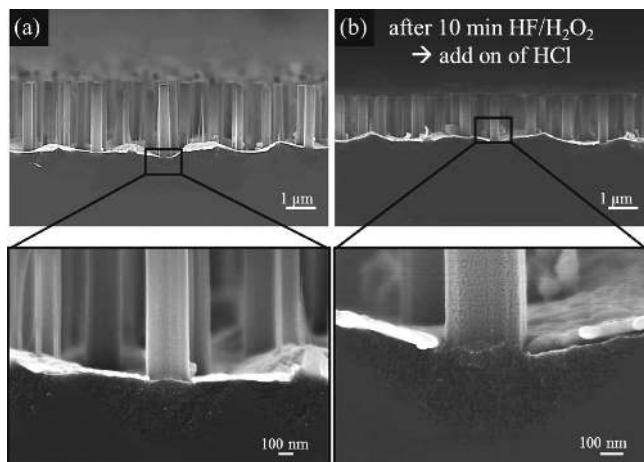

Figure 5. Ag$^+$ ions eliminated by means of HCl leading to a termination of the etching process. (a) Conventional etching process, no addition of HCl, wires reach their normal length. (b) Addition of HCl after 10 min. The wires cease to form.

without adding HCl and Figure 5b after adding HCl. In the second case, the NWs are much shorter: the HCl eliminated the ions from the solution and the MACE process terminated.

■ DISCUSSION

We may now formulate the model describing the charge transport during MACE. Our model of the etching process is based on two prerequisites: (i) a source of electronic holes for the oxidation of Si and (ii) a direct contact with the electrolyte

(HF, H$_2$O$_2$) necessary for etching off the oxidized Si surface. The dissolution mechanism can be described in analogy to the anodic etching by the following overall reaction[19]

$$Si + \frac{n}{2}H_2O_2 + 6HF \rightarrow nH_2O + H_2SiF_6 + \frac{4-n}{2}H_2\uparrow$$

(7)
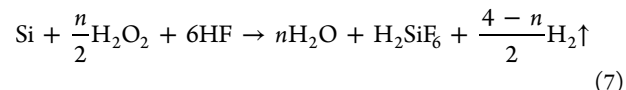
where $n = 2$ for formation of pSi and $n = 4$ for electropolishing.

Our model for the mass transport at the Si/metal interface region based on the experimental findings is the following: the etching process forms a thin pSi layer for the exchange of reactants and byproducts of the reaction, see Figure 6a.[27] However, this porous layer, which allows the mass transport, is at the same time a strong obstacle for the charge transport, as
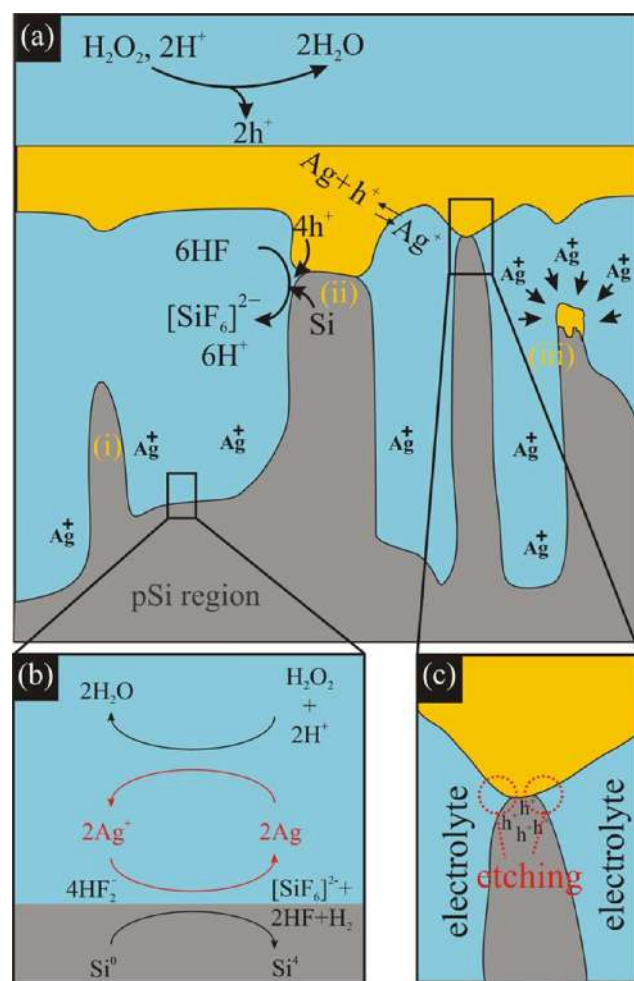
Figure 6. (a) Schematic representation of the charge transport process during MACE with contiguous metal films under the formation of pSi (gray) catalyzed by mobile Ag$^+$ ions in the electrolyte. Through the porous medium, the electrolyte can diffuse beneath the metal (yellow). (b) Electronic holes are transported to the interface pSi/bulk-Si by the redox couple Ag/Ag$^+$, which acts as a redoxmediator. First, the H$_2$O$_2$ is reduced at the Ag particle to H$_2$O. Hence, electrons are extracted from the Ag, which are delivered from the underlying Si. This leads to an injection of holes in the Si and to the formation of elementary Ag. That means the Ag is cyclically reduced and oxidized. This is how the charges are transported. (c) There are still some direct contact points of the pore walls and the Ag tips. Here, two prerequisites for an electropolishing are fulfilled: a high current density of holes due to the direct contact to the metal film and a direct contact to the electrolyte. The electropolishing takes place.

4306

dx.doi.org/10.1021/am400510f | ACS Appl. Mater. Interfaces 2013, 5, 4302−4308

pSi is electrically isolating. On the other hand, the electrolyte is a conducting medium penetrating through the pores to the etching fronts. Experiments where the metal catalyst was spacially separated from the etching site showed an electrochemical dissolution and a redeposition of the metal on the Si surface. Thus, a metal redox couple of a solid elementary phase and mobile ions are responsible for the charge diffusion through the electrolyte. In the case of Ag, the reaction is the following

$$Ag^+ \rightarrow Ag(s) + h^+ \tag{8}$$

Holes are generated at the surface of the metal film through the reduction of H_2O_2, which leads to a formation of Ag^+-ions. These ions diffuse through the porous layer and are deposited on the sidewalls of the Si as elementary Ag particles. The holes generated in this reduction are absorbed in the Si oxidation process according to eq 6. At the redeposited Ag particles, H_2O_2 reduction is catalyzed just like on the original Ag film and the Ag particles can be mobilized again. This mechanism of charge transfer via eq 8 is then cyclically repeated in the further formation of pSi, see Figure 6b. The etching rate of the pSi can be estimated to be between 3 nm/s (slightly doped Si) and 13 nm/s (highly doped Si) and can be taken as a measure for the average local current density.[19,30] For our etching solution, the critical etching rate amounts to around 31 nm/s. Thus, according to the model of Chartier et al.[19] and Smith et al.[31] only pSi could form in this regime. After the pSi is formed, the metal layer has only small point-like contacts with the remaining porous Si skeleton, as shown in Figure 2b and the corresponding scheme in Figure 6c. In these points, the current density reaches locally values high enough for the electropolishing to take place (that means a field-induced injection at the silver tip[32]). There appears also a direct contact of the metal to the electrolyte as well as an abundant supply of electronic holes from the H_2O_2 reduction at the surface of the metal film. This is similar to the case of etching with metal particles. Therefore an etching of the remaining Si occurs preferentially at the contact of Ag and Si, which leads to a further movement of the Ag layer into the Si substrate. The SiNWs are formed.

CONCLUSION

The charge transport mechanism during MACE of SiNWs was investigated in a series of experiments, and a plausible model has been suggested to answer the fundamental question of how the electrical charges necessary for the oxidation of Si can penetrate to the etching fronts. The model can be summarized as follows: (i) Starting from the lithographic openings in the metal film, a pSi layer forms between the metal film and the Si surface (etching front 1). The pSi layer is the fundamental transport medium of the etching solution to the etching fronts. (ii) The charges necessary for the etching of the pSi originate through the catalytic reaction of the oxidative agent H_2O_2 at the surface of the metal. The charge transport proceeds in an electrochemical way in the pores of Si beneath the film mediated by the redox system Ag/Ag^+. (iii) Only in the direct contact of the Si pore walls and the metal additional electrical transport without a redox mediator is possible. In such regions, the electropolishing of the pSi occurs and leads to the sinking in of the metal film into the substrate.

METHODS

SiNWs were fabricated based on the technique published by Huang et al.[11] This method combines nanosphere lithography for the production of a suitable lithography mask, plasma etching with MACE. Different commercial Si substrates with doping levels from 1×10^{14} to 1×10^{19} cm^{-3} (p- as well as n-doped) have been used as starting material. In a first step, the Si substrate has to be masked with a monolayer of monodisperse hexagonally closed packed polystyrene (PS) spheres (commercially available from "Microparticles GmbH" as a 10 wt % solution). In order to obtain hydrophilic and chemical homogeneous Si surfaces, the Si substrate was first cleaned with RCA-I, which involved a 15 min etch in H_2O_2 (30 wt %), NH_4OH (25 wt %), and H_2O (volume ratio of 1:1:5) at 80 °C. Afterward, the cleaned substrates were rinsed with deionized water, and a monolayer of PS spheres was deposited on the Si surface by a Langmuir–Blodgett technique. In the next step, the diameter of the PS spheres was reduced by oxygen plasma etching using a process pressure of 0.06 mbar with a pure oxygen flow of 160 sccm. Subsequent to the plasma etching, a silver film was deposited on the substrate covered with the PS mask. The thickness of the Ag layer amounted to 60 nm in all experiments. After lifting-off the PS spheres, an Ag layer with a hexagonal array of openings was formed and served as the catalyst in the subsequent MACE step. The etching solution was composed of 5.65 mol/L HF and 0.10 mol/L H_2O_2. The resulting structure is an array of SiNWs.

To characterize the topography and the composition of the samples, we carried out scanning electron microscopy (SEM) using a XL30 ESEM-FEG Philips. Imaging with secondary electrons (SE) provides details about the topology of the sample's surface and morphology. Backscattered electron (BSE) imaging can provide information about the composition of the structures, because the intensity of the BSE signal is determined by the atomic number of the investigated material. Therefore, heavy electrons (e.g., Ag) are stronger scattered than light electrons (e.g., Si) and appear consequently with a higher contrast in the BSE image. For a detailed investigation of the internal structure and composition of the NWs, tansmission electron microscopy (TEM) using a JEOL JEM 4010 was performed. For this purpose, we have prepared electron-transparent cross-section samples by the standard preparation of mechanical grinding, polishing, dimpling, and Ar ion milling.

ASSOCIATED CONTENT

Ⓢ Supporting Information

Figure S1: SE and BSE images of unstructured Si substrates (B-doped Si (100)-wafer, 10^{15} cm^{-3}) etched with the HF/H_2O_2 solution with an addition of varying concentration of Ag^+ ions. This material is available free of charge via the Internet at http://pubs.acs.org.

AUTHOR INFORMATION

Corresponding Author
*E-mail: ngeyer@mpi-halle.de. Phone: +49 (0)345 5582-976.

Notes
The authors declare no competing financial interest.

ACKNOWLEDGMENTS

REFERENCES

(1) Schmidt, V.; Riel, H.; Senz, S.; Karg, S.; Riess, W.; Gösele, U. *Small* **2005**, *2*, 85−88.
(2) Goldberger, J.; Hochbaum, A. I.; Fan, R.; Yang, P. *Nan. Lett.* **2006**, *6*, 973−977.

(3) Tian, B.; Zheng, X.; Kempa, T. J.; Fang, Y.; Yu, N.; Yu, G.; Huang, J.; Lieber, C. M. *Nature* **2007**, *449*, 885−890.

(4) Hochbaum, A. I.; Chen, R.; Delgado, R. D.; Liang, W.; Garnett, E. C.; Najarian, M.; Majumdar, A.; Yang, P. *Nature* **2008**, *451*, 163−168.

(5) Peng, K. Q.; Xu, Y.; Wu, Y.; Yan, Y. J.; Lee, S. T.; Zhu, J. *Small* **2005**, *1*, 1062−1067.

(6) Garnett, E. C.; Yang, P. *J. Am. Chem. Soc.* **2008**, *130*, 9224−9225.

(7) Hwang, Y. J.; Boukai, A.; Yang, P. *Nano Lett.* **2009**, *9*, 410−415.

(8) Cui, Y.; Wei, Q.; Park, H.; Zhang, W.; Lee, S.-T. *Science* **2001**, *293*, 1289−1292.

(9) Patolsky, F.; Zheng, G.; Lieber, C. M. *Nat. Protoc.* **2006**, *1*, 1711−1723.

(10) Wolfsteller, A.; Geyer, N.; Ngyuen-Duc, T.-K.; Das Kanungo, P.; Zakharov, N. D.; Reiche, M.; Erfurth, W.; Blumtritt, H.; Werner, P.; Gösele, U. *Thin Solid Films* **2010**, *518*, 2555−2561.

(11) Huang, Z.; Fang, H.; Zhu, J. *Adv. Mater.* **2007**, *19*, 744−748.

(12) Huang, Z.; Shimizu, T.; Senz, S.; Zhang, Z.; Zhang, X.; Lee, W.; Geyer, N.; Gösele, U. *Nano Lett.* **2009**, *9*, 2519−2525.

(13) Huang, Z.; Geyer, N.; Werner, P.; De Boor, J.; Gösele, U. *Adv. Mater.* **2011**, *23*, 285−308.

(14) Geyer, N.; Huang, Z.; Fuhrmann, B.; Grimm, S.; Reiche, M.; Nguyen-Duc, T.-K.; de Boor, J.; Leipner, H. S.; Werner, P.; Gösele, U. *Nano Lett.* **2009**, *9*, 3106−3110.

(15) Tsujino, K.; Matsumura, M. *Electrochem. Solid-State Lett.* **2005**, *8*, C193−C195.

(16) Peng, K. Q.; Fang, H.; Hu, J.; Wu, Y.; Zhu, J.; Yan, Y.; Lee, S. T. *Chem.—Eur. J.* **2006**, *12*, 7942−7947.

(17) Peng, K. Q.; Hu, J. J.; Yan, Y. J.; Wu, Y.; Fang, H.; Xu, Y.; Lee, S.-T.; Zhu, J. *Adv. Funct. Mater.* **2008**, *18*, 3026−3035.

(18) Li, X.; Bohn, P. W. *Appl. Phys. Lett.* **2000**, *77*, 2572−2574.

(19) Chartier, C.; Bastide, S.; Lévy-Clément, C. *Electrochim. Acta* **2008**, *53*, 5509−5516.

(20) Chattopadhyay, S.; Li, X. L.; Bohn, P. W. *J. Appl. Phys.* **2002**, *91*, 6134−6140.

(21) Lee, C. L.; Tsujino, K.; Kanda, Y.; Ikeda, S.; Matsumura, M. *J. Mater. Chem.* **2008**, *18*, 1015−1020.

(22) Xia, X. H.; Ashruf, C. M.; French, P. J.; Kelly, J. J. *Chem.. Mater.* **2000**, *12*, 1671−1678.

(23) Peng, K. Q.; Wu, Y.; Fang, H.; Zhong, X. Y.; Xu, Y.; Zhu, J. *Angew. Chem., Int. Ed.* **2005**, *44*, 2737−2742.

(24) Asoh, H.; Sakamoto, S.; Ono, S. *J. Colloid Interface Sci.* **2007**, *52*, 2894−2898.

(25) Lehmann, V. In *Electrochemistry of Silicon: Instrumentation, Science, Materials, and Applications*; Wiley-VCH: Weinheim, Germany, 2002.

(26) Föll, H.; Christophersen, J.; Carstensen, J.; Hasse, G. *Mater. Sci. Eng., R* **2002**, *39*, 93−141.

(27) Geyer, N.; Fuhrmann, B.; Huang, Z.; De Boor, J.; Leipner, H. S.; Werner, P. *J. Phys. Chem. C* **2012**, *116*, 13446−13451.

(28) Lehmann, V.; Gösele, U. *Appl. Phys. Lett.* **1991**, *58*, 856−858.

(29) Peng, K. Q.; Yan, Y. J.; Gao, S. P.; Zhu, J. *Adv. Funct. Mater.* **2003**, *13*, 127−132.

(30) Huang, Z.; Geyer, N.; Liu, L. F.; Li, M. Y.; Zhong, P. *Nanotechnology* **2010**, *21*, 465301−465306.

(31) Smith, R. L.; Collins, S. D. *J. Appl. Phys.* **1992**, *71*, R1−R22.

(32) Sedlewicz, P. G.; Onley, R. E.; Kannewurf, C. R. *Solid-State Electron.* **1964**, *7*, 225−235.